Bioelectrochemistry 140 (2021) 107835

Contents lists available at ScienceDirect

Bioelectrochemistry

journal homepage: www.elsevier.com/locate/bioelechem

A novel tool for the adsorption of dsDNA: Electrochemical reduction of Pd nanoparticles onto reduced-keratin particles extracted from wool wastes

Meryem Kalkan Erdoğan, Gözde Aydoğdu Tığ *, Mehmet Saçak *

Ankara University, Faculty of Science, Department of Chemistry, Ankara, Turkey

ARTICLE INFO

Article history:
Received 2 April 2021
Received in revised form 25 April 2021
Accepted 29 April 2021
Available online 5 May 2021

Keywords:
Waste wool fabric
Reduced-keratin particles
Pd nanoparticles
dsDNA adsorption
Electrochemical biosensor

ABSTRACT

This work outlines the fabrication of a novel electrochemical platform for the dsDNA adsorption, using one of the most sustainable materials, wool fabric waste, and Pd^{2+} ions. To develop a functional material with a significant adsorption capability, the waste wool was subjected to the chemical reduction process, and the keratin-SH (KerSH) particles were extracted in powder form. These particles were used in the adsorption of Pd^{2+} ions by monitoring with the UV–vis spectra. The dispersion of the KerSH-Pd^{2+} particles was subsequently drop-casted onto a glassy carbon electrode (GCE) and electrochemically reduced to the GCE/KerSH-PdNPs composite by chronoamperometry at −0.4 V for 500 s. It was found that the KerSH particles were self-assembled by revealing chemically attractive NH_2 groups after the electrochemical PdNPs deposition. A GCE/KerSH-PdNPs composite was then employed in the electrochemical dsDNA detection by Differential Pulse Voltammetry (DPV), using the oxidation signals of guanine and adenine bases at 0.8 V and 1.2 V, respectively. Accordingly, relatively stable, repeatable, and reproducible dsDNA adsorption was ensured through the positively charged-NH_2 groups of KerSH-PdNPs. This finding reveals the potential of textile waste for various electrochemical applications, such as DNA biosensors for environmental, pharmaceutical, and medicinal fields.

1. Introduction

Wool is a keratinous type of animal fiber that has been one of the most preferred natural textile materials in conventional clothing applications. Its excellent properties, such as biocompatibility, relatively low cost, easy maintenance, high mechanical strength, warm-keeping, and good dyeability, have been an indispensable source for the preparation of apparel fabrics. These properties of wool also appeal to other scientific and technological fields, where especially require biocompatibility and biological activity [1], such as ocular surface reconstruction [2], tissue regeneration [3], cell growth, migration, and proliferation [4,5]. With the contribution of other functional agents, such as metal nanoparticles and some conductive additives, the role of the wool in the other biomedical or environmental-based fields, such as antibacterial wound dressing [6], flexible sensor development [7], and humidity sensing [8] can also be increased. Therefore, the use of wool wastes generated during the preparation of clothing products from such valuable material can play a significant role in revealing the potential of wool for promising application areas. Starting from that idea, we inspired by the possible waste fabric management of the textile manufacturers and evaluated the out-of-use wool fabric crops as a 2D-modifier layer on the GCE for the dsDNA adsorption.

Although the aforementioned superior properties of wool, the presence of disulfide crosslinks on its external layers may cause a hindrance during the application of a hydrophilic surface modification onto the wool. Thus, the researchers have dissipated this limitation by the cleavage of disulfide links, using many different wet chemical extraction methods, including solely reduction or subsequent reconstruction of newly formed —SH groups using another sulfur-containing molecule [9–14], and hydrolysis [15,16] in the literature. Among them, the reduction of wool keratin can be found advantageous in enabling high KerSH extraction yields by tuning the reduction bath and the requirement of environmentally less hazardous ingredients and less energetic apparatus. To improve the accessibility of the keratin functional groups and increase their affinity to the hydrophilic reagents, we also preferred the reduction of wool before the experiments.

The incorporation of metal nanoparticles (MeNPs), such as AuNps, AgNps, and PdNPs, onto the various support substrates,

* Corresponding authors.
E-mail addresses: gaydogdu@science.ankara.edu.tr (G. Aydoğdu Tığ), sacak@science.ankara.edu.tr (M. Saçak).

https://doi.org/10.1016/j.bioelechem.2021.107835
1567-5394/

enables the formation of versatile materials due to the desired properties of the selected metals, such as high surface area, high chemical stability, high conductivity, and size-dependent electrochemical property [17]. With the help of this, the MeNPs decorated surfaces can be used in different application fields, such as heterogeneous organic catalysts [18], dye decolorization [19], electrochemical sensing development platforms [20–22], tissue engineering [23], surface-enhanced Raman scattering [24], and drug delivery [25]. Among them, the electrochemical methods have been frequently appealed to the researchers due to their unique properties, such as low cost, rapid response, high selectivity and sensitivity, low limit of detection, non-requirement of additional separation steps, and miniaturized devices [26–29]. For these methods, the development of a biocompatible and functional electrochemical platform for biosensing applications has been a requirement due to non-cytotoxic and stable micro-environment creation for the biomolecules, such as nucleic acids and enzymes. For that reason, many studies have been reported including a biopolymer such as a chitosan [30], gelatin [31], poly(amino acids) [32], in the presence or absence of these MeNPs for biomolecule detection/adsorption purposes.

In this work, we utilized an out-of-use waste wool fabric to prepare reduced-KerSH particles, and the Pd^{2+} ions were adsorbed onto these particles. The as-prepared material was then used as the electrode modifier through drop-casting on the surface, and the Pd^{2+} ions were further electrochemically reduced via chronoamperometry technique. To the best of our knowledge, no reports have been present in the literature regarding the use of KerSH-PdNPs composite matrix as the modification platform for electrochemical biomolecule sensing. Only in a few studies, the environmental humidity sensing [8,33], strain sensing [34], and transducer for human motion sensing [35] investigations were performed in the presence of keratin derivatives. Considering the main target of these researches, our study can be found quite different in terms of many points. First, we transformed a waste wool material into a helpful modification agent; second, we electrochemically decorated the KerSH surface with PdNPs, we intended to self-organize the functional groups of keratin. Finally, we utilized this cost-effective material as a suitable platform for the dsDNA adsorption.

2. Materials and methods

2.1. Materials

The wool fabrics were provided from Yünsa Co., Turkey. The out-of-use wool fabric crops that occurred after precise cutting with a scissor were employed in the experiments after washing in 1 g/L ECE reference detergent containing water bath (1/50 w/V) at 40 °C for 30 min. Double-stranded DNA from fish sperm was purchased from Serva Company (Germany). The chemicals, including thioglycolic acid (TGA), $NaHS{\cdot}xH_2O$, urea, thiourea, HCl (37%), NaOH, $PdCl_2$ (60% Pd), KCl, sodium acetate, acetic acid, and ethyl alcohol, were all provided from Sigma Aldrich (Turkey) and directly used in the experiments without subjecting to a purification process.

2.2. Methods

2.2.1. Extraction of KerSH from waste wool by the reduction method

According to a literature method based on the previous studies, the extraction of KerSH from the wool was carried out [11,36]. Accordingly, 1.000 g wool fabric wastes were taken into a two-necked reaction flask containing 50 mL 2.0 M urea or 1.5 M thiourea solution and mixed at 35 °C under a nitrogen atmosphere. After adding 1.000 g NaHS or TGA to the medium, the pH was adjusted to 10.5, and the reaction was maintained at 35 °C for 24 h under a nitrogen atmosphere. At the end of 24 h, the viscous solution was separated by filtration to remove the unreacted-wool scales, thoroughly washed with distilled water, acidified with 6.0 M aqueous HCl solution until the pH reached 4–5, and finally, the reduced KerSH particles were precipitated. Then, the isolated particles were thoroughly washed with distilled water and dried in a vacuum oven until reaching a constant weight. Dried KerSH particles were also gently crumbled in an agar mortar to obtain more fine particles. The yield (%) of the KerSH particles was calculated gravimetrically by considering the weights of initial waste wool and weighed keratin particles. The structures of wool and KerSH particles are represented in Scheme 1.

2.2.2. Adsorption of Pd^{2+} onto KerSH particles

0.120 g of fine KerSH particles that were previously grounded in the mortar were transformed to the pellet samples in 1.3 cm diameter under 8 kN pressure. Then, these pellets were suspended in the 2 mL specific concentrations of aqueous Pd^{2+} solutions (0.02, 0.04 M, 0.08 M) prepared in the aqueous HCl solutions (0.2 M, 0.4 M, 0.8 M) at ambient temperature for 120 min. At the end of the time, the KerSH-Pd^{2+} complexes were isolated from the solution, dispersed well in the distilled water to remove the unreacted Pd^{2+} ions, centrifuged at 4000 rpm, and finally dried on a glass watch at 50 °C until reaching the constant weight. The adsorbed Pd amount was determined gravimetrically, considering the weight increase and the KerSH particles' initial weight. The Pd adsorption values in (%) and (g Pd/g wool) units of the samples were also calculated considering the changes in the UV–vis absorption spectra of the Pd+2 solutions λ_{max}: 435 nm.

2.2.3. Electrode modification steps

Firstly, the bare GCE surface was polished using 3.0, 1.0, and 0.25 μm alumina slurries on a polishing pad several times. After each polishing, the electrode was sonicated in ethanol (50% v/v) and ultra-pure water for 5 min, respectively. To modify the GCE surface, first, the diluted dispersion of Pd^{2+}/KerSH particles was prepared. For that purpose, first, 1 mL KerSH dispersion extracted by NaHS (6 mg/mL in ethyl alcohol) was taken to 4 mL ethyl alcohol. To this dispersion, 1.28 mL of Pd^{2+} (5 mg/mL in 0.5 M HCl) was dropwise added for the adsorption. The concentrations of KerSH dispersion and Pd^{2+} were set at 1 mg/mL. Then the mixture was stirred at ambient temperature for 120 min. At the end of the 120 min, the adsorbed Pd^{2+} content of the keratin-SH particles was calculated as 63.67 mg Pd/1 g KerSH through UV–vis measurement. The volume of that dispersion was set at 10 mL using ethyl alcohol, and its composition was 0.6 mg/mL KerSH and 0.038 mg/mL Pd^{2+}. Then, the as-prepared 10 μL of KerSH-Pd^{2+} dispersion was drop-casted onto the GCE surface and dried at 60 °C for 15 min. The KerSH-Pd^{2+} drop-casted GCE electrode (GCE/KerSH-Pd^{2+}) was then immersed into a 0.1 M KCl solution to electrodeposit Pd nanoparticles by chronoamperometry a constant potential of −0.4 V (*vs.* Ag/AgCl) for 500 s. The obtained composite electrode was rinsed with ultra-pure water and denoted as GCE/KerSH-PdNPs. For comparison, the GCE/KerSH electrode was also obtained by a drop-casting method with 10 μL of Ker-SH solution. The GCE/PdNPs/KerSH electrode, which was used for the comparison, was also prepared by first electrodeposition of PdNPs at −0.4 V for 500 s (0.04 mg/mL), followed by drop-casting of 10 μL of KerSH dispersion (0.4 mg/mL). The schematic representation for the modified electrode is illustrated in Scheme 2.

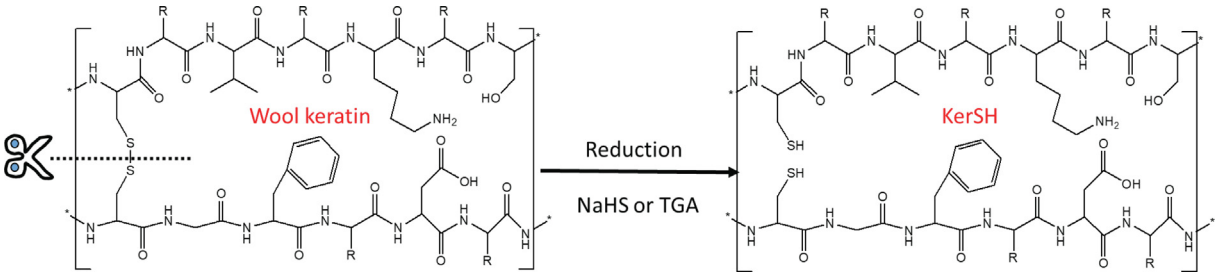

Scheme 1. The extraction of KerSH particles from out-of-use-wool fabric wastes through reduction method.

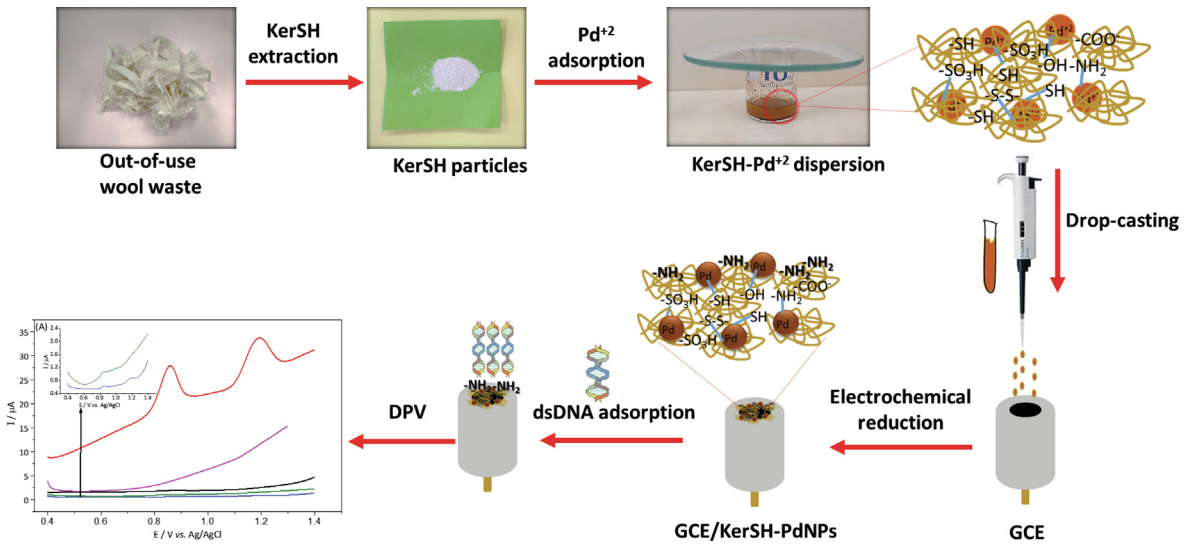

Scheme 2. Schematic representation for the preparation of the modified GCE electrode.

2.3. Characterization

The ATR-FTIR spectra were obtained using Perkin Elmer 100 FTIR spectrometer. UV–vis spectra of the samples were recorded by Shimadzu 1700 Spectrophotometer. The surface elemental composition of the GCE electrode before and after the modification was revealed by the samples' XPS spectra, taken with the PHI 5000 VersaProbe instrument using an Al monochromatic X-ray anode. The narrow scan spectra of certain elements were fitted using the most appropriate function in the Origin Lab Pro 9. The SEM micrographs were monitored by QUANTA 400F Field Emission SEM Instrument after the application of the Au-Pd coating process. The contact angle measurements of the GCE surfaces were performed with an Attension Theta Lite Optical Contact Angle Measurement Instrument using the Sessile Drop method. Electrochemical studies were recorded with an Autolab PGSTAT 302 N potentiostat equipped with a FRA32M module (Eco Chemie, The Netherlands) and connected to a traditional three-electrode cell; a GCE (ϕ = 3 mm, BASi, USA) as working electrode, an Ag/AgCl (BASi, USA) as reference electrode and a platinum wire (BASi, USA) as the auxiliary electrode.

Electrochemical properties of the prepared-electrodes were conducted by cyclic voltammetry (CV) and electrochemical impedance spectroscopy (EIS) techniques in a 0.1 M KCl solution containing 5.0 mM $Fe(CN)_6^{3-/4-}$. The EIS experiments were carried out at the open-circuit applied potential, the frequency range was 100 kHz–0.01 Hz, and the amplitude was 5 mV. The differential pulse voltammetry (DPV) measurements were performed between (+0.4) and (+1.2) V (*vs.* Ag/AgCl) in 0.5 M acetate buffer solution (ABS) containing 0.1 M NaCl. The DPV conditions were: pulse amplitude, 50 mV; scanning speed, 15 mV s^{-1}; pulse time, 0.02 s; voltage step, 3 mV.

3. Results and discussion

3.1. Pd^{2+} adsorption studies

As the first attempt for the adsorption of Pd^{2+} onto the KerSH particles, the reducing agent used in the reduction bath was determined. For that purpose, two different reducing agents capable of attacking the disulfide links of wool, including NaHS and TGA, were employed in the experiments, in the presence or absence of urea derivatives, for the dissolution of the keratin. After the extraction of KerSH using NaHS and TGA with or without urea/thiourea, these particles were examined in the adsorption Pd^{2+} in the aqueous HCl medium for 120 min. The changes in the UV–Vis absorption spectra of the Pd^{2+} solutions containing different KerSH particles were monitored, and the results are comparatively given in Fig. 1. When the untreated wool was suspended in the Pd^{2+} solution, no significant change was obtained in the characteristic Pd^{2+} absorption band at λ_{max} 435 nm (Fig. 1(A)). This may imply that no interaction was ensured between wool and Pd^{2+} due to the wool structure's strong intermolecular interactions. When the KerSH particles extracted by TGA/thiourea were suspended in the Pd^{2+} solution (Fig. 1(B)), the yellow color of the Pd^{2+} solution slightly took a darker shade λ_{max} value shifted to ~391 nm, and the intensity of the absorption band remarkably increased. These findings may also indicate the formation of other Pd-TGA complexes [37] due to the possible presence of TGA residues on the KerSH particles that

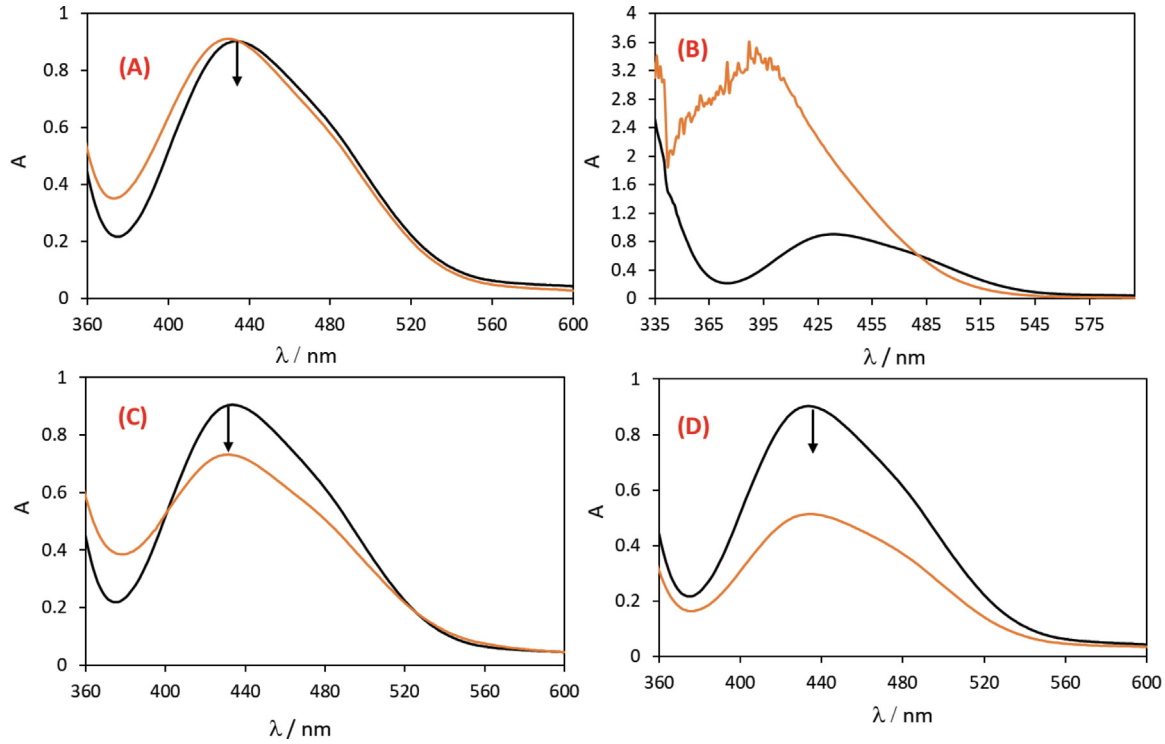

Fig. 1. The changes in UV–vis absorption spectra of Pd^{2+} solutions with reducing agents used in the extraction of KerSH (A) untreated wool, (B) TGA-thiourea, (C) NaHS-urea, and (D) NaHS. The black lines are the blank Pd^{2+} solutions and the orange lines adsorption after 120 min.

would act as a bidental ligand through O and S atoms [38]. Unlike that of TGA-thiourea, the KerSH particles that NaHS-urea and NaHS extracted showed a marked decrease in the Pd^{2+} absorption value and color shade of the solution (Fig. 1(C) and (D)), and this decrease was more pronounced, especially for solely NaHS employed-KerSH particles (43.0% Pd^{2+} adsorption). It can be suggested that the KerSH particles that NaHS extracted did not cause the formation of separate complex particles, as observed for the TGA, but possibly provided embedding into the KerSH structure, through strong interaction between the functional groups. Accordingly, further investigations continued with the KerSH particles extracted by NaHS and NaHS-urea.

The changes in Pd^{2+} adsorption (%) values of the KerSH particles extracted by NaHS-urea and NaHS were monitored with Pd^{2+} concentrations, utilizing time-dependent UV–vis spectra. The individual results are represented in Figs. 2 and 3. As seen from both figures, the Pd^{2+} adsorption (%) values of both KerSH particles showed an increasing tendency with time and reached saturation at 120 min. The Pd^{2+} adsorption (%) values of both KerSH particles also followed a decreasing trend with the Pd^{2+} concentration. At 120th min, the highest Pd^{2+} adsorption (%) values were recorded 82.3% and 84.3% for NaHS-urea and NaHS, respectively, when 0.02 M of Pd^{2+} was used for both particles.

When these results were evaluated considering the reducing agents used in the extraction process, the NaHS-extracted particles showed relatively higher Pd^{2+} adsorption (%) values than that of the NaHS-urea binary system the investigated Pd^{2+} concentrations. The underlying fact of this finding may be correlated with the presence of excess keratolytic urea that facilitates the dissolution of the keratin structure in the aqueous alkaline medium [39] and causes the by-product lanthionine formation [40], which is induced by the disulfide desulfurization degradation [41]. Thus, excess urea in the extraction medium may have caused a decrease in the required functional groups of KerSH that would have an affinity to the Pd^{2+}.

The Pd^{2+} amounts in g Pd/g wool are also comparatively depicted in Fig. S1 at the changing Pd^{2+} concentrations. Although the highest Pd^{2+} adsorption was obtained using 0.02 M Pd^{2+}, both of the particles possessed the highest Pd^{2+} adsorption amounts when the concentration was increased. Since the amount of KerSH particles, and thus, the numbers of active functional groups are higher than that of the Pd^{2+} in the medium at 0.02 M concentration, the functional groups might not have fully occupied by relatively fewer numbers of Pd^{2+} ions. With the increment of the concentration, the amounts of Pd^{+2} incorporated into the KerSH structures also increased and reached saturation. Thus, after the further increase of concentration to 0.08 M, the Pd adsorption amounts of NaHS-employed KerSH particles did not show a remarkable change from that of 0.04 M. But the Pd adsorption amount of KerSH particles prepared by the NaHS-urea binary system slightly decreased due to the presence of excess urea residues.

3.2. ATR-FTIR spectra

The structural changes in the wool keratin after the NaHS reduction were revealed from the samples' ATR-FTIR spectra in Fig. 4. In the spectrum of untreated wool, the bands at 3275, 2931, 1640, and 1534 cm^{-1} correspond to the stretching vibrations of the peptide structure, including N—H, aliphatic C—H, C=O (amide I), and bending vibration of N—H (amide II), respectively [10,42]. While the bands at 1396 and 1072 cm^{-1} are attributed to the respective stretching vibrations of the axial deformation of C=O and S—O groups [43], the band around 1240 cm^{-1} is addressed to the stretching vibrations of C—N and C—O, and N—H and O=C—N bending vibrations of the amide III structure [44,45]. After the reduction of wool and extraction of KerSH with NaHS, it was observed that the characteristic bands of amide II (1534 cm^{-1}) and amide III (~1240 cm^{-1}) shifted to the lower wavenumbers, including 1517 cm^{-1} and 1233 cm^{-1}, but the amide

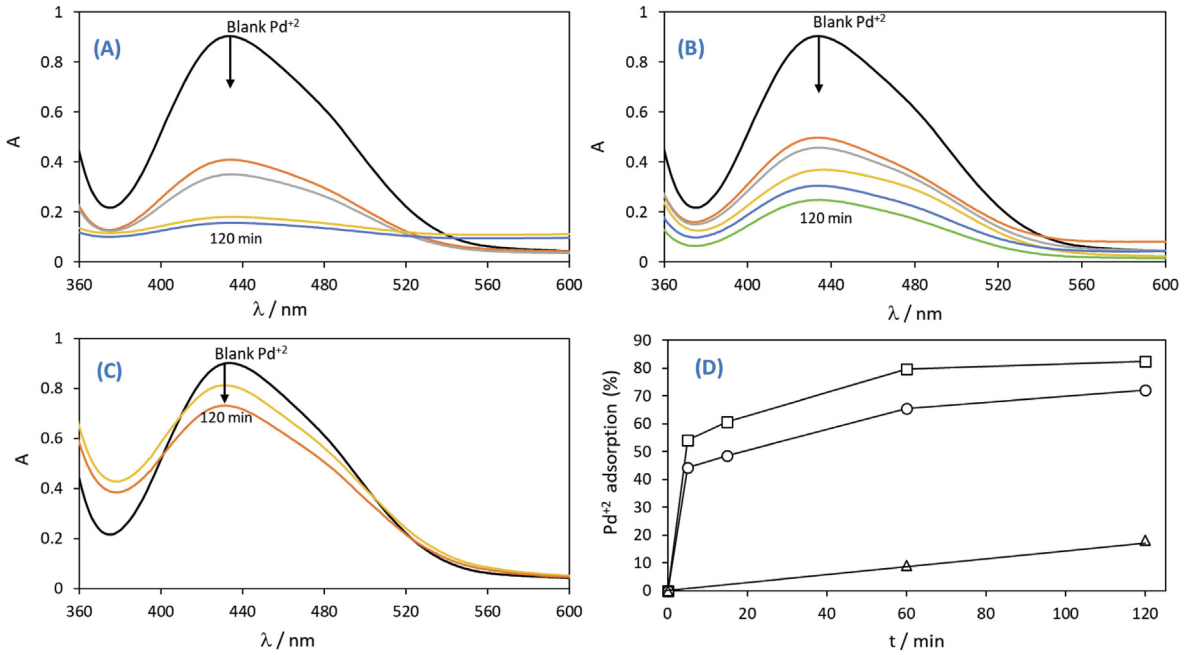

Fig. 2. The changes in time dependent-UV–Vis absorption spectra of Pd^{2+} solutions with Pd^{2+} concentration using NaHS-urea as the reducing agents for the KerSH, (A) 0.02 M, (B) 0.04 M, and (C) 0.08 M Pd^{2+}, (D) The changes in Pd^{2+} adsorption yields (%) of the respective Pd^{2+} solutions with time, 0.02 M (square), 0.04 M (circle), and 0.08 M (triangle).

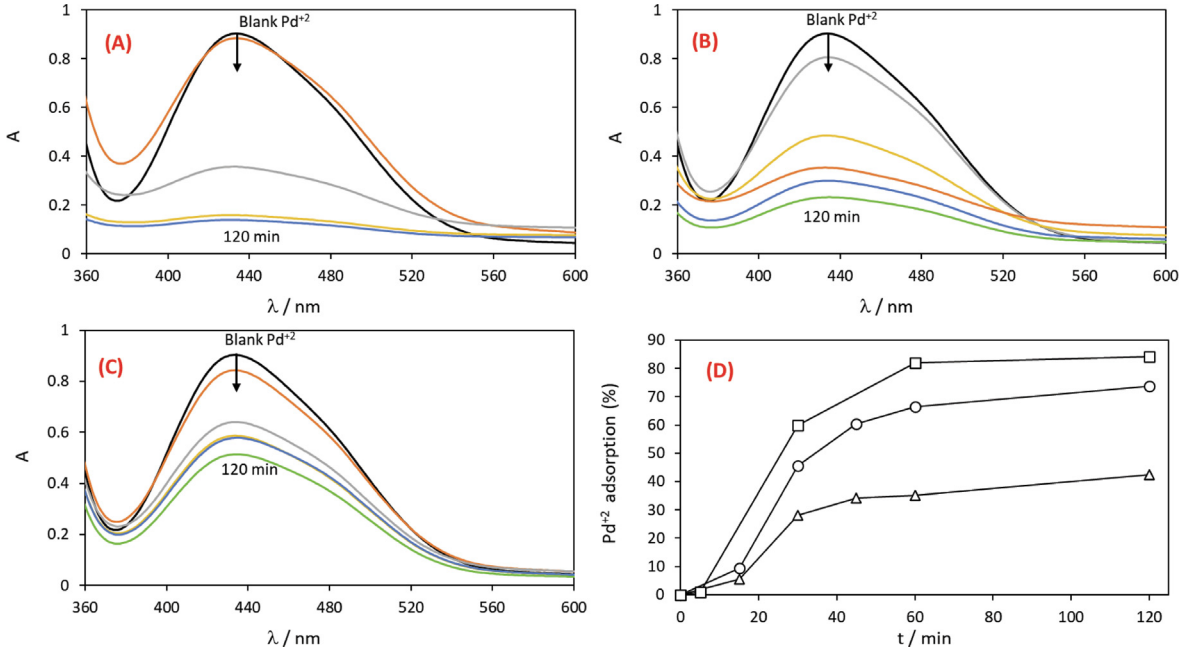

Fig. 3. The changes in time dependent-UV–Vis absorption spectra of Pd^{2+} solutions with Pd^{2+} concentration using NaHS as the reducing agent for KerSH, (A) 0.02 M, (B) 0.04 M, and (C) 0.08 M Pd^{2+}, (D) The changes in Pd^{2+} adsorption yields (%) of the respective Pd^{2+} solutions with time, 0.02 M (square), 0.04 M (circle), and 0.08 M (triangle).

I band (1640 cm^{-1}) arose at a higher wavenumber (1646 cm^{-1}). A new band was also detected at 830 cm^{-1}, corresponds to the 1,4-disubstituted benzene unit present in the tyrosine structure [46]. This finding suggests that the wool's protein structure may have remarkably altered by the extraction process, such as a conformational change in the α-helix (~1650 cm^{-1}) and β-sheet structures (~1630 cm^{-1}). The possible changes in the positions of these bands indicate the change in the seconder structure of the keratin arrangement [14,44,46–48]. Accordingly, taking into account the observed- shift in the amide I band, it can be said that the structure of KerSH particles became more likely to the α-helix structure after the extraction process.

3.3. Electrochemical characterization

To investigate the electrochemical performance of the prepared KerSH-PdNPs composite modified GCE, the cyclic voltammogram (CVs) and EIS measurement were recorded in the redox probe of $Fe(CN)_6^{-3/-4}$. Fig. 5(A) exhibits the CVs of bare, GCE/KerSH-Pd^{2+}, and GCE/KerSH-PdNPs electrodes in the potential range from

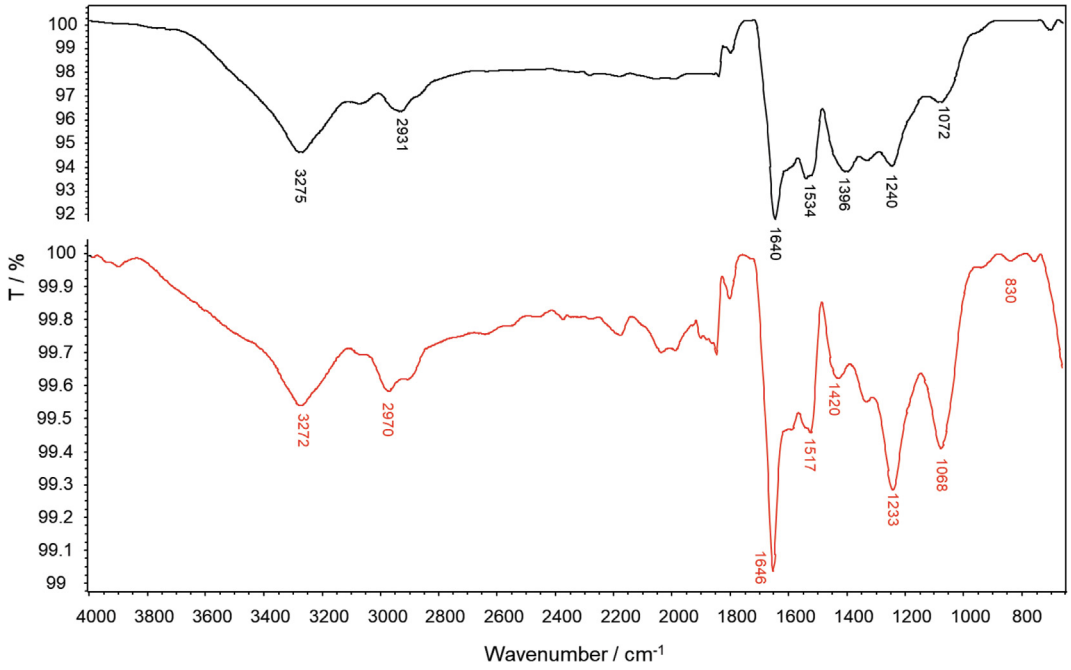

Fig. 4. ATR-FTIR spectra of untreated-wool fabrics (black line) and KerSH particles (red line) obtained using NaHS.

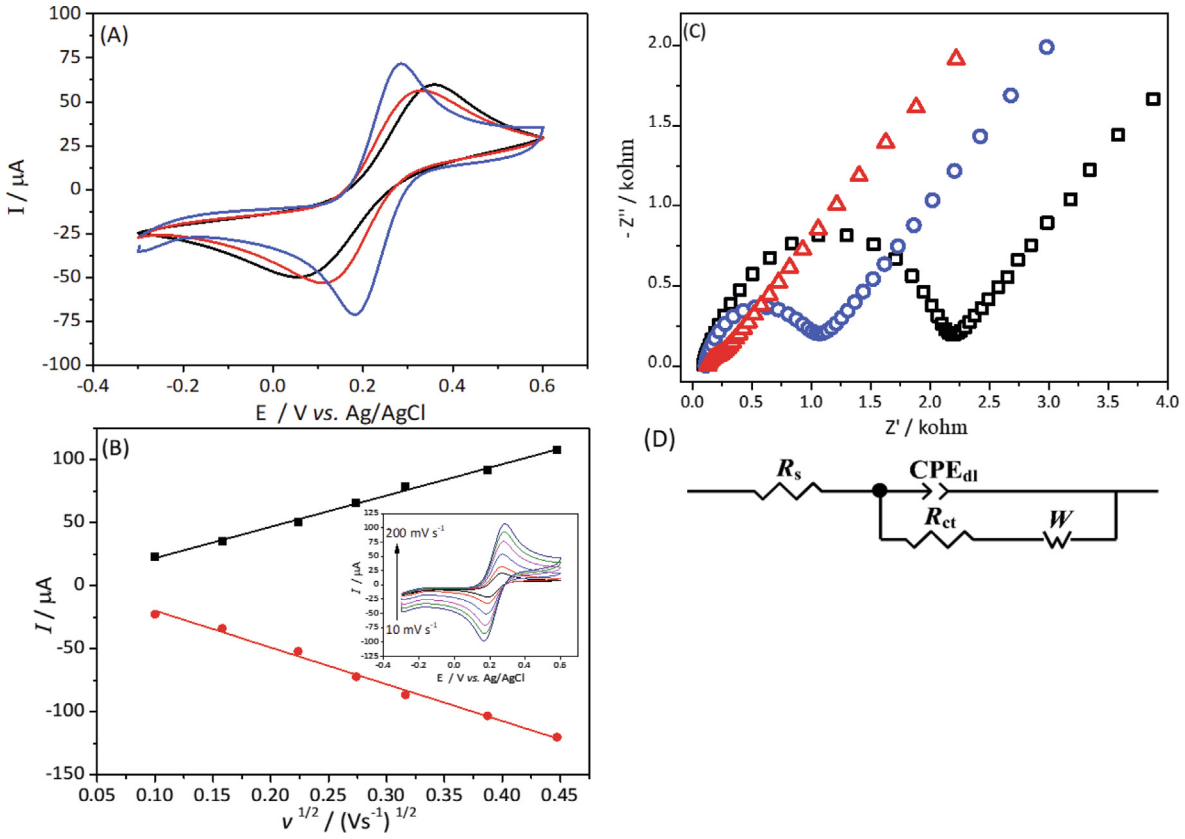

Fig. 5. (A) CVs (B) The plot of peak current against the square root of scan rate (ip$_a$ R^2 = 0.995, ipc R^2 = 0.992, inset; CV curves of GCE/KerSH-PdNPs electrode with various scan rate between 10 and 200 mV s^{-1}) (C) The Nyquist curves of (a) bare GCE (black curve), (b) GCE/KerSH-Pd^{2+} (blue curve), and (c) GCE/KerSH-PdNPs (red curve) electrodes at scan rate 50 mV s^{-1} in 1.0 M KCl solution containing 5.0 mM $Fe(CN)_6^{3-/4-}$. (D) The equivalent circuit model for bare and modified electrodes.

−0.3 V +0.6 V at a scan rate of 50 mV s^{-1}. As shown in the figure, a well-defined redox peak couple with the peak separation (ΔE_p) of 0.273 V was observed for bare GCE (curve a), while GCE/KerSH-Pd^{2+} electrode showed lower anodic and cathodic peak currents due to the non-conductive nature of KerSH particles. However, ΔE_p value was calculated as 0.190 V, which shows a relatively

higher electron transfer rate between ferri-ferrocyanide redox probes at the non-reduced composite than bare GCE. After the electrochemical reduction of PdNPs, a significant increment in the oxidation and reduction peak signals and a decrease in the ΔE_p value (0.095 V) were obtained. These results indicate that the Pd^{2+} ions were successfully reduced to PdNPs onto the GCE surface and the electron transfer rate considerably increased in the presence of PdNPs in the KerSH particles.

The effect of the scan rate on the GCE/KerSH-PdNPs electrodes was monitored by CV at various scan rates, as exhibited in Fig. 5 (B). The anodic and cathodic peak currents increased with the increasing scanning speed in the range of 10–200 mV s^{-1} and a linear correlation was observed between the electrochemical signals of the redox probe and the square root of scan rate demonstrating the reversible, diffusion-controlled redox process of the Fe^{+3}/Fe^{+2} redox couple [49].

The electroactive surface area of the developed GCE/KerSH-PdNPs electrode can be calculated from the peak response of the redox probe via Randles–Sevcik equation at a scan rate of 25 mV s^{-1}:

$$i_p = \left(2.69 \times 10^5\right) n^{3/2} A C D^{1/2} \nu^{1/2} \quad (1)$$

where i_p represents the peak current (A), n is the number of electrons transferred in the redox reaction (n = 1), A corresponds to the electroactive surface area of the electrode (cm^2), D is the diffusion coefficient (6.67 × 10^{-6} cm^2 s^{-1} for ferricyanide) [50]. C is the redox probe concentration (mol cm^{-3}), and ν represents the scan rate (V s^{-1}).

The electroactive surface area of the GCE/KerSH-Pd^{2+} and GCE/KerSH-PdNPs electrodes were calculated as 0.087 cm^2 and 0.131 cm^2 at a scan rate of 25 mV s^{-1} using the Randles–Sevcik equation (Eq. (1)). This value was much higher than that of bare GCE (0.070 cm^2). The results appeared that the GCE modified with KerSH-PdNPs composite improved the electron transfer process between the redox probe solution and the surface of the modified

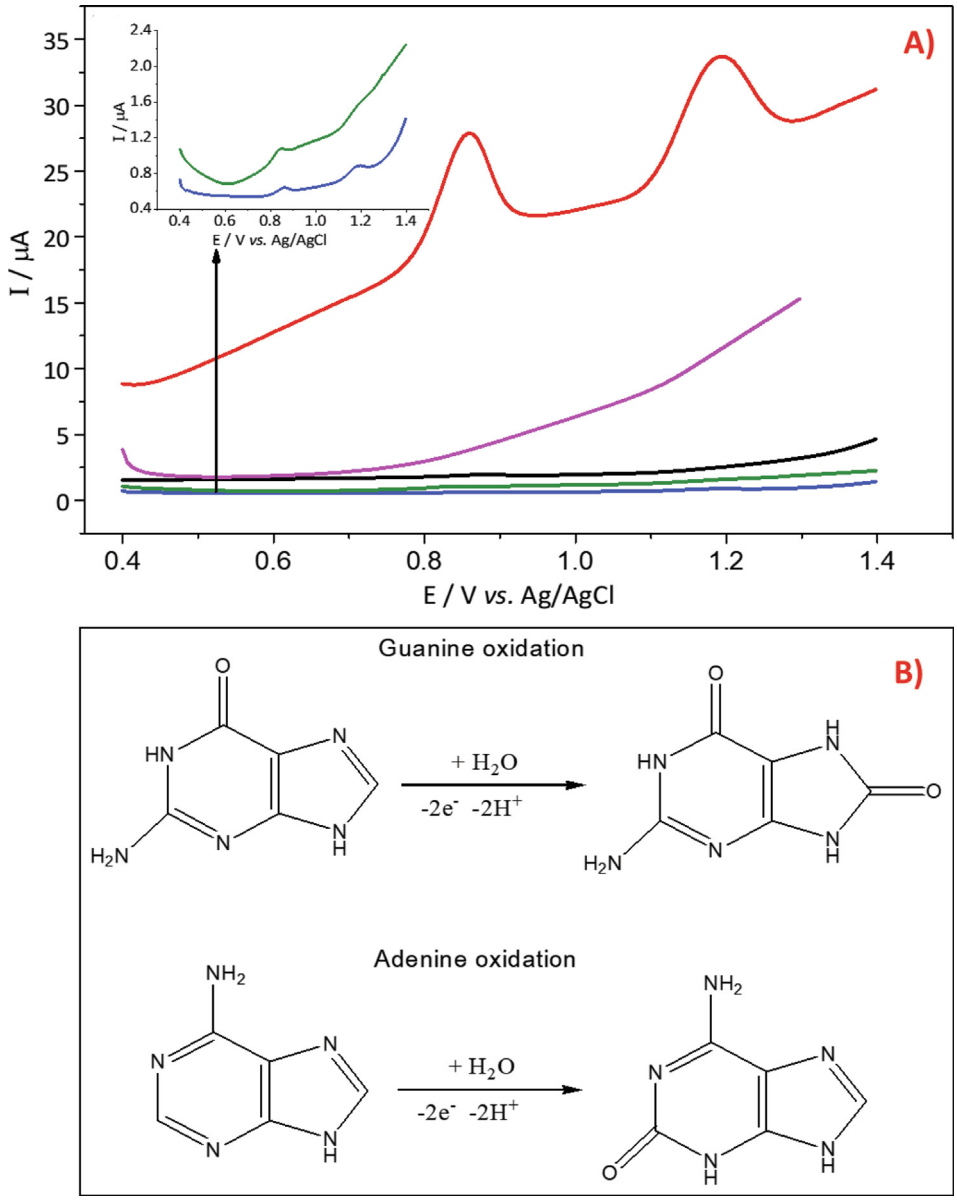

Fig. 6. (A) DPVs of 25 µg/mL dsDNA at the GCE/KerSH (a) (black curve), GCE/PdNPs (b) (red curve), GCE/PdNPs/KerSH (c) (blue curve) GCE/KerSH-Pd^{2+} (d) (pink curve) and GCE/KerSH-PdNPs (e) (green curve) (0.5 M ABS, pH 4.8) (B) The possible electro-oxidation mechanism for guanine and adenine.

electrode due to the electrocatalytic activity and the electrical conductivity of PdNPs [51,52].

Electrochemical impedance spectroscopy (EIS) is an effective technique to explain the interfacial properties such as charge transfer, diffusion, and conductivity of the modified electrodes [53,54]. Fig. 5(C) represents the Nyquist plot of bare and modified electrodes, and the equivalent circuit used to fit these curves is also given in Fig. 5(C). A typical Nyquist plot includes a semicircle and a linear part. At high frequencies, the semicircle part corresponds to the electron transfer resistance (R_{et}), and at low frequencies, the linear part expresses the diffusion behavior of the electrode/electrolyte interface [55]. The R_{et} values of bare GCE, GCE/KerSH-Pd^{2+}, and GCE/KerSH-PdNPs electrodes were 2070 Ω, 890 Ω, and 77.6 Ω, respectively. These results reveal that the prepared GCE/KerSH-PdNPs electrode shows high electron transfer kinetics in the redox probe solution and serves as an appropriate conducting substrate to immobilize several biomolecules. This can be attributed to the enhanced surface area for charge transfer and positively charged GCE/KerSH-PdNPs substrate structure.

The electrodeposition time and potential are the crucial parameters that control the distribution of nanoparticles [56]. To evaluate the influence of the electroreduction potential and time of PdNPs, the oxidation signals of guanine and adenine bases were monitored by the DPV technique in 0.5 M ABS (pH 4.8). As shown in Fig. S2(A), the oxidation peak currents increased with decreasing potential from −0.1 to −0.4 V and then remained almost constant. The electro-reduction time was also studied in the range of 100 s and 600 s. As shown in Fig. S2(B), the maximum oxidation peaks for both guanine and adenine appeared at 500 s. Therefore, the optimum electro-reduction potential and time for PdNPs were selected as −0.4 V and 500 s, respectively.

3.4. dsDNA adsorption studies

The prepared GCE/KerSH-PdNPs electrode is considered an efficient and stable platform for biomolecule immobilization. Therefore, dsDNA was immobilized onto the surface of GCE/KerSH-PdNPs via the passive adsorption method. For this purpose, 25.0 μg/mL dsDNA solution is prepared in 0.5 M acetate buffer solution, and the GCE/KerSH-PdNPs electrode was immersed into a vial containing dsDNA solution for 15 min. Then, differential pulse voltammograms (DPVs) were recorded in the potential range from +0.4 V to +1.4 V in 0.5 M ABS (pH 4.8). Fig. 6(A) shows DPVs of 25.0 μg/mL dsDNA immobilized at GCE/KerSH (a), GCE/PdNPs (b), GCE/PdNPs/KerSH (c) GCE/KerSH-Pd^{2+} (d) and GCE/KerSH-PdNPs (e). After the modification of GCE with KerSH and PdNPs/KerSH separately, it was observed that the characteristic guanine and adenine bases peaks of dsDNA have poorly been detected at +0.8 V and +1.2 V, respectively, indicating that these modification steps are insufficient for determining dsDNA. As shown in curves b and d, no electrochemical responses were also detected towards dsDNA at the GCE/PdNPs and GCE/KerSH-Pd^{2+} electrodes due to the absence and unavailability of free —NH_2 groups of KerSH particles, respectively. The guanine and adenine nucleobases of dsDNA immobilized at the electrode surface undergo irreversible electrochemical oxidation processes, and the sensing mechanism was given in Fig. 6(B) [57,58]. After the electrochemical reduction of GCE/KerSH-PdNPs (curve e), the guanine and adenine anodic peaks were remarkably defined at higher current intensity values. These results can be attributed to the formation of high interaction of negatively charged –PO_4^{3-} groups of dsDNA with –NH_2 groups of KerSH particles as possible results of the developed composite's enhanced orientation at the electrode surface.

To find the most appropriate electrochemical response for dsDNA oxidation, different concentrations from 5.0 to 50 μg/mL of dsDNA were adsorbed onto the GCE/KerSH-PdNPs surface. The oxidation peak currents increased with increasing dsDNA concentrations until 25.0 μg/mL dsDNA (Fig. 7(A)) and then reached a plateau due to the saturation of the electrode surface by dsDNA molecules. Thus, 25.0 μg/mL was selected as the optimum concentration for further experiments. The effect of dsDNA adsorption time was also evaluated between 5 and 30 min. As shown in Fig. 7(B), the oxidation peaks of guanine and adenine increased to 15 min then nearly unchanged. Therefore, 15 min was chosen as the most suitable adsorption time for dsDNA loading.

The repeatability GCE/KerSH-PdNPs electrode was evaluated by calculating relative standard deviations (RSD) obtained from the guanine oxidation signals of seven successive DPV measurements at the same electrode in 0.5 M ABS (pH 4.8). The RSD% value of the guanine oxidation peak currents was found as 2.16%. The reproducibility results of seven independently prepared electrodes were estimated as 3.75%. The initial DPV current response of the fabricated electrode for 10 and 35 days retained approximately 97.1% and 92.9%, respectively. These results reveal that the GCE/KerSH-PdNPs electrode possesses high repeatability, reproducibility, and storage stability for the electrochemical sensing of dsDNA.

3.5. XPS results

To determine the structural changes of KerSH-Pd^{2+} particles after an electrochemical reduction on the GCE electrode, the XPS spectra of the samples were recorded, and the results are listed in Fig. 8. The binding energies and relevant abundance values, calculated by considering the peak areas, are also provided in Table S1. In the GCE/KerSH-Pd^{2+} electrode spectrum, the characteristic two Pd_{3d} peaks were determined at 335.7 eV and 341.1 eV,

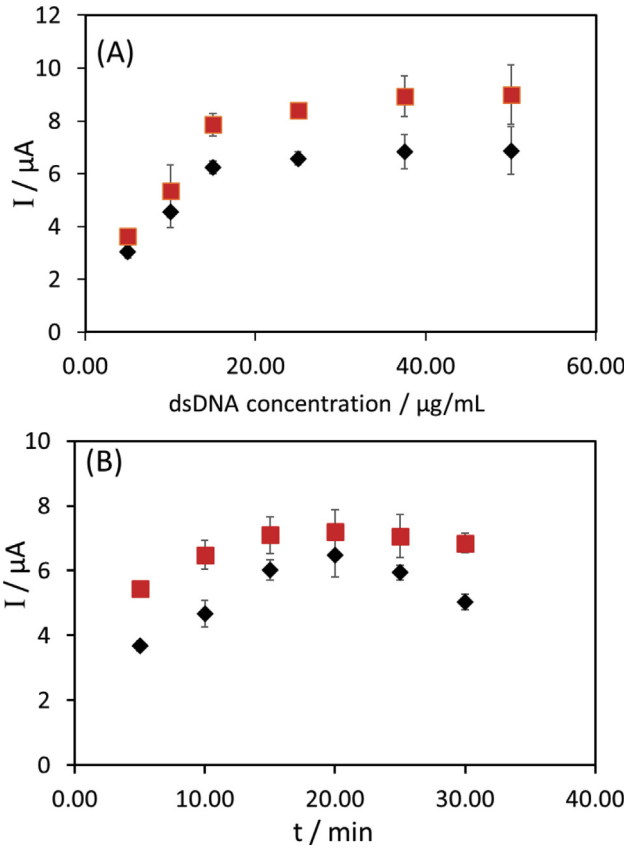

Fig. 7. Effect of (A) concentration and (B) adsorption time of dsDNA on the DPV signal of the guanine (black) and adenine (red) at the GCE/KerSH-PdNPs composite (0.5 M ABS, pH 4.8).

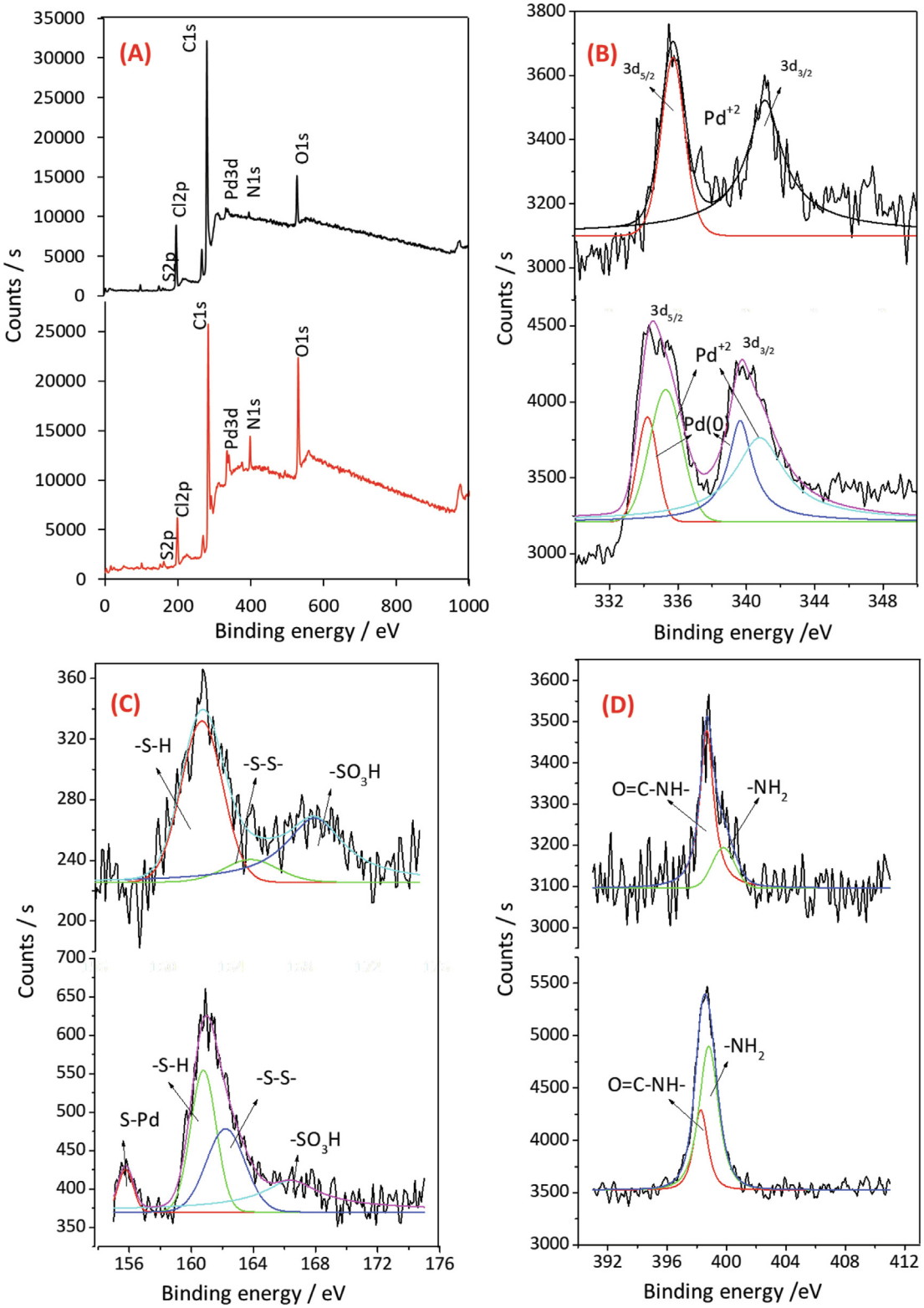

Fig. 8. (A) wide scan XPS survey spectra of GCE/KerSH-Pd^{2+} (black line) and GCE/KerSH-PdNPs (red line), narrow scan XPS spectra of (B) Pd_{3d} GCE/KerSH-Pd^{2+} (upper) and GCE/KerSH-PdNPs (bottom), C) S_{2p} GCE/KerSH-Pd^{2+} (upper) and GCE/KerSH-PdNPs (bottom), and (D) N_{1s} GCE/KerSH-Pd^{2+} (upper) and GCE/KerSH-PdNPs (bottom).

which correspond to the $Pd3d_{5/2}$ and $Pd3d_{3/2}$ of Pd^{2+} ions [59]. The GCE/KerSH-PdNPs also gave two different $Pd3d_{5/2}$ and $Pd3d_{3/2}$ peaks, including 334.2 and 335.3 eV and 339.6 340.8 eV, of which the lowest peaks prove the noble PdNPs formation on the GCE electrode [60]. When the other narrow scan spectra are evaluated in general, it can be seen that both of the samples possess characteristic bond types that were previously identified for wool keratin in the literature, including —SH, —S—S—, —SO_3H for S_{2p} spectrum and O═C—NH— and NH_2 for N_{1s} spectrum, respectively [59,61]. Due to the application of a disulfide cleavage reduction process, it was

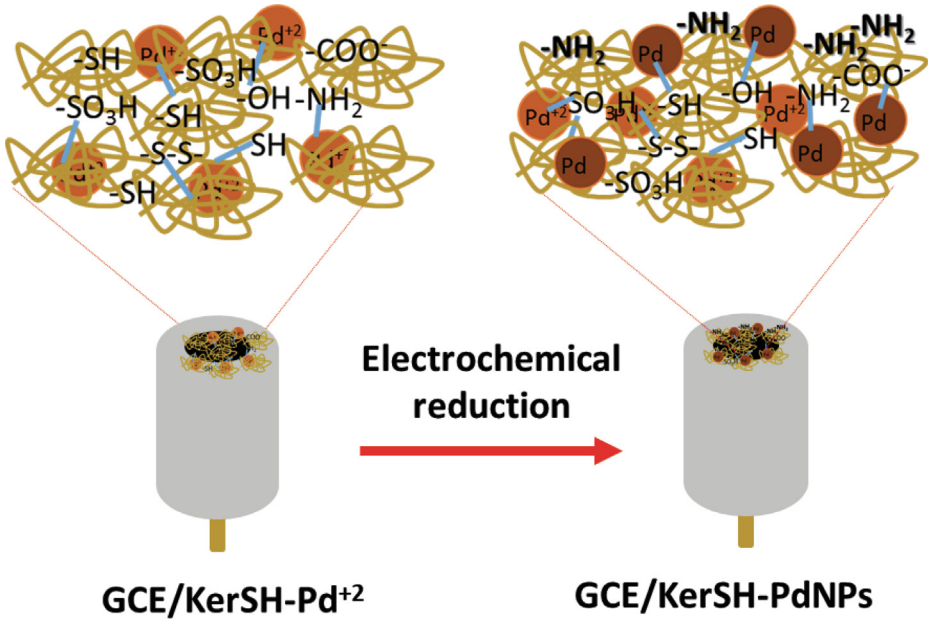

Scheme 3. The possible assembly of KerSH particles after the electrochemical reduction of PdNPs.

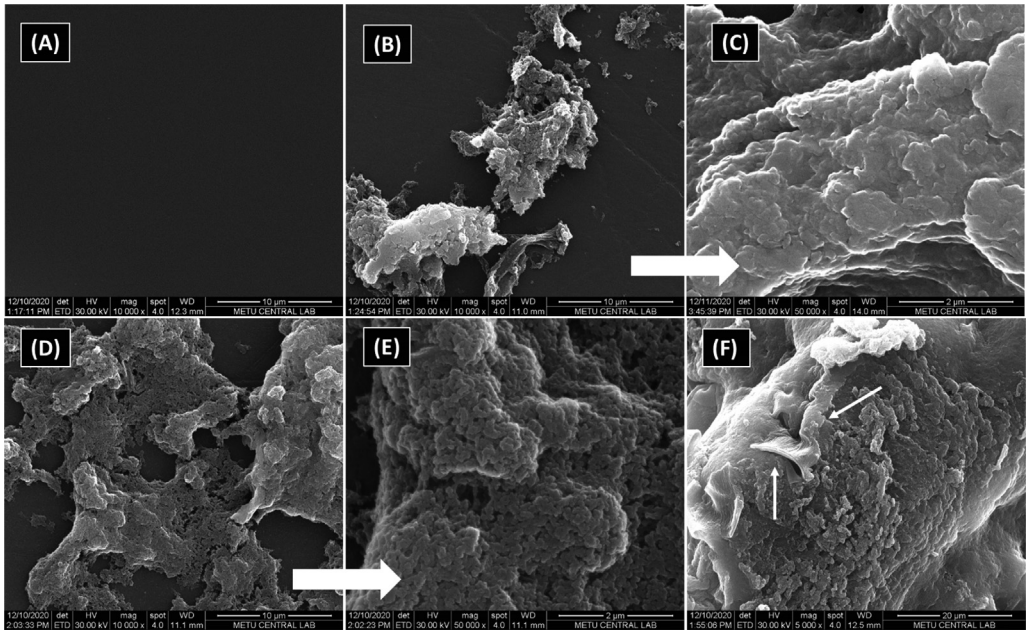

Fig. 9. SEM micrographs of (A) bare GCE electrode, (B) and (C) GCE/KerSH-Pd^{2+}, (D) and (E) GCE/KerSH-PdNPs composite, and (F) DNA-adsorbed GCE/KerSH-PdNPs composite.

observed that the relative abundance values, especially those of —SH and —S—S— (Table 1S), remarkably differed in both of the samples, compared to the literature [61].

When the narrow scan spectra of the samples were compared with each other, while no remarkable change was obtained in the —S—S— relative abundance values of the samples (Fig. 8(C)), the values of —NH_2, —SH, and —SO_3H markedly changed after the electrochemical PdNPs reduction (Fig. 8(C) and (D)). Besides, a new peak was deconvoluted at 155.8 eV in the S_{2p} spectrum of GCE/KerSH-PdNPs composite, which may be assigned to the presence of the S-Pd^{2+} bonding type. This implies that some Pd^{2+} ions may also be coordinated to the KerSH structure in addition to the PdNPs formation. Accordingly, the possible assembly of the KerSH-PdNPs on the GCE surface is depicted in Scheme 3.

3.6. SEM micrographs

The surface morphological properties of the samples that were deposited onto the GCE electrode are comparatively presented in Fig. 9. As seen from the micrograph of the GCE/KerSH-Pd^{2+} (Fig. 9 (B)), it was observed that the bulky KerSH-Pd^{2+} particles were aggregated on the surface of the GCE electrode with a non-

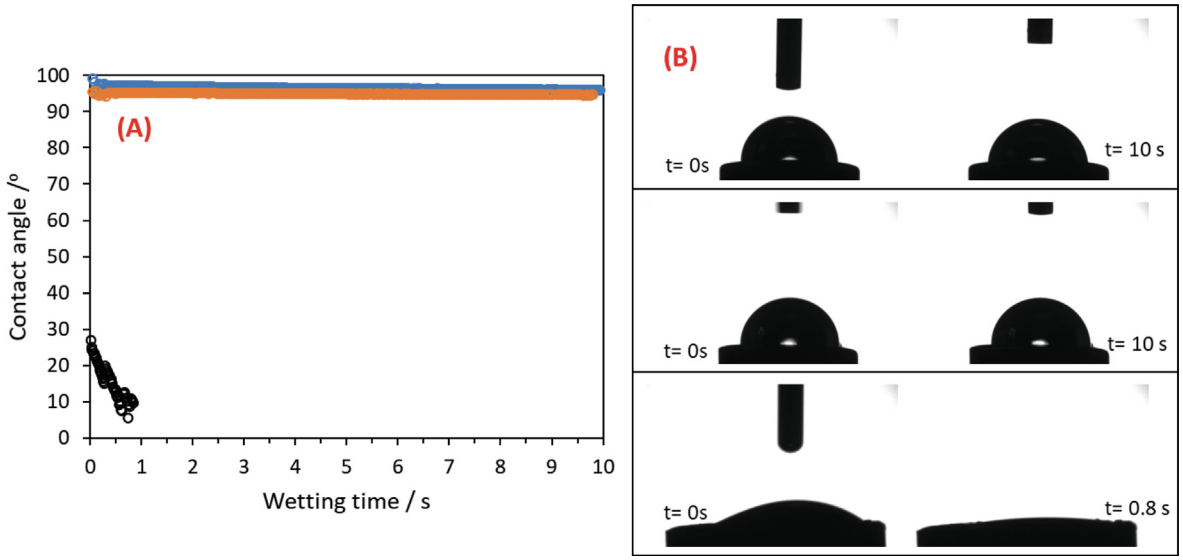

Fig. 10. (A) Change in contact angle values of bare GCE electrode (blue), GCE/KerSH-Pd^{2+} (orange) and GCE/KerSH-PdNPs composite (black) with wetting time, (B) the optical images of the water droplets on the GCE (up), GCE/KerSH-Pd^{2+} (middle), and GCE/KerSH-PdNPs (bottom) surfaces at the initial and end of the measurement.

homogenous distribution. The texture of the GCE/KerSH-Pd^{2+} surface has a nonporous compact structure, which is more evident from the micrograph taken at the higher magnification (Fig. 9(C)). After the electrochemical reduction of Pd nanoparticles, it was noticed that the surface of the GCE electrode took a more densely covered appearance, whose globular PdNPs can be distinguished on the surface. The compact structure of the KerSH took a rather loose and porous form and previously embedded Pd was re-organized for coating the KerSH particles (Fig. 9(E)). After the dsDNA adsorption onto the GCE/KerSH-PdNPs (Fig. 9(F)), the composite's surface became flattened, which is easily understood from the flaky sites marked by the arrows. The micrograph also gives the impression of dsDNA has adhered to the relatively compact KerSH sections of the composite, indicating that a strong interaction could be ensured between dsDNA and KerSH.

3.7. Contact angle results

The changes in the surface wetting characteristic of the bare GCE electrode, GCE/KerSH-Pd^{2+}, and GCE/KerSH-PdNPs composite were determined from the water contact angle measurements that are comparatively depicted in Fig. 10. Due to the possible manufacturing process of GCE and the application of polishing [62], the GCE electrode displayed a hydrophobic behavior with an average of 96.5° ± 0.6 water contact angle value for 10 s. After the drop-casting of KerSH-Pd^{2+} onto the GCE, the contact angle value was measured as an average of 94.9° ± 0.2, indicating that the GCE surface's wetting characteristic was not remarkably altered. Unlike the GCE/KerSH-Pd^{2+} surface, the GCE/KerSH-PdNPs surface's contact angle significantly decreased to 30.4° with a decreasing trend with time, and the surface was thoroughly wetted with a contact angle of 9.8° at 0.8 s (Fig. 10(B)). This implies that the electrochemical reduction of PdNPs led to an increment in the GCE hydrophilicity, as the possible results of the presence of KCl salt on the surface and increase in the polar functional groups content of the KerSH. This finding can also be evidenced by the XPS findings, such as the increased NH_2 and SO_3H intensity values in the narrow scan spectra of the GCE/KerSH-PdNPs composite.

4. Conclusions

It was demonstrated with this work that environmentally-sustainable and abundant out-of-use wool fabric wastes turn in provide into valuable material for the preparation of an electrochemical sensing platform for dsDNA in the existence of PdNPs. To reach this goal, the employment of facile chemical procedures, including the reduction of wool with the NaHS and adsorption of Pd^{2+} ions onto the KerSH particles, was observed to yield the required environment for the dsDNA adsorption. The FTIR spectra results confirmed the structural changes in the keratin chains, and UV–vis spectra revealed the desired Pd^{2+} adsorption onto the KerSH. After casting these KerSH-Pd^{2+} particles onto the GCE, the chronoamperometry technique afforded the decoration of PdNPs onto the surface. The XPS findings evidenced the self-assembling of KerSH particles, leading to an increase in NH_2 and SO_3H functional groups and the formation of PdNPs, after the electrochemical reduction. The most noteworthy result of the study was the satisfactorily highly stable (after 35 days, activity 92.9%), repeatable (2.16%), and reproducible (3.75%) adsorption of dsDNA onto the GCE/KerSH-PdNPs. This concludes that the developed electrode modification process may pioneer the use of waste textile products as the functional platform for electrochemical biosensor applications.

Declaration of Competing Interest

The authors declare that they have no known competing financial interests or personal relationships that could have appeared to influence the work reported in this paper.

Appendix A. Supplementary material

Supplementary data to this article can be found online at https://doi.org/10.1016/j.bioelechem.2021.107835.

References

[1] J.G. Rouse, M.E. Van Dyke, A review of keratin-based biomaterials for biomedical applications, Materials 3 (2) (2010) 999–1014.
[2] M. Borrelli, N. Joepen, S. Reichl, D. Finis, M. Schoppe, G. Geerling, S. Schrader, Keratin films for ocular surface reconstruction: evaluation of biocompatibility in an in-vivo model, Biomaterials 42 (2015) 112–120.
[3] H. Zhang, H. Ma, R. Zhang, K. Wang, J. Liu, Construction and characterization of antibacterial PLGA/wool keratin/ornidazole composite membranes for periodontal guided tissue regeneration, J. Biomater. Appl. 34 (9) (2020) 1267–1281.
[4] C. Su, J.-S. Gong, J.-P. Ye, J.-M. He, R.-Y. Li, M. Jiang, Y. Geng, Y. Zhang, J.-H. Chen, Z.-H. Xu, J.-S. Shi, Enzymatic extraction of bioactive and self-assembling wool keratin for biomedical applications, Macromol. Biosci. 20 (9) (2020) 2000073.
[5] A. Patrucco, F. Cristofaro, M. Simionati, M. Zoccola, G. Bruni, L. Fassina, L. Visai, G. Magenes, R. Mossotti, A. Montarsolo, C. Tonin, Wool fibril sponges with perspective biomedical applications, Mater. Sci. Eng., C 61 (2016) 42–50.
[6] C.D. Tran, F. Prosenc, M. Franko, Facile synthesis, structure, biocompatibility and antimicrobial property of gold nanoparticle composites from cellulose and keratin, J. Colloid Interface Sci. 510 (2018) 237–245.
[7] A.B. Patil, M. Zhaohui, R. Wu, L. Ma, Z. Xu, S. Chenyang, Q. Wu, Q. Liu, Y. Zhang, L. Youhui, Tailoring the meso-structure of gold nanoparticles in keratin-based activated carbon toward high-performance flexible sensor, Nano-Micro Lett. 12 (1) (2020).
[8] M. Natali, A. Campana, T. Posati, E. Benvenuti, F. Prescimone, D.O.S. Ramirez, A. Varesano, C. Vineis, R. Zamboni, M. Muccini, A. Aluigi, S. Toffanin, Engineering of keratin functionality for the realization of bendable all-biopolymeric micro-electrode array as humidity sensor, Biosens. Bioelectron. 141 (2019) 111480.
[9] R. Asquith, N. Leon, Chemical reactions of keratin fibers, in: Chemistry of Natural Protein Fibers, Springer, 1977, pp. 193–265.
[10] P. Kakkar, B. Madhan, G. Shanmugam, Extraction and characterization of keratin from bovine hoof: A potential material for biomedical applications, SpringerPlus 3 (1) (2014) 596.
[11] H. Matsuda, M. Takahashi, K. Shinoda, S. Kikyotani, H. Inagaki, Process for producing reduced keratinous substances using urea or thiourea, Google Patents, 1979.
[12] A. Kuzuhara, T. Hori, Reduction mechanism of tioglycolic acid on keratin fibers using microspectrophotometry and FT-Raman spectroscopy, Polymer 44 (26) (2003) 7963–7970.
[13] K.Y. Lee, S.J. Kong, W.H. Park, W.S. Ha, I.C. Kwon, Effect of surface properties on the antithrombogenicity of silk fibroin/S-carboxymethyl kerateine blend films, J. Biomater. Sci. Polym. Ed. 9 (9) (1998) 905–914.
[14] K. Wang, R. Li, J.H. Ma, Y.K. Jian, J.N. Che, Extracting keratin from wool by using l-cysteine, Green Chem. 18 (2) (2016) 476–481.
[15] M. Zoccola, A. Aluigi, A. Patrucco, C. Vineis, F. Forlini, P. Locatelli, M.C. Sacchi, C. Tonin, Microwave-assisted chemical-free hydrolysis of wool keratin, Text. Res. J. 82 (19) (2012) 2006–2018.
[16] P. Bhavsar, M. Zoccola, A. Patrucco, A. Montarsolo, G. Rovero, C. Tonin, Comparative study on the effects of superheated water and high temperature alkaline hydrolysis on wool keratin, Text. Res. J. 87 (14) (2017) 1696–1705.
[17] R. Sardar, A.M. Funston, P. Mulvaney, R.W. Murray, Gold Nanoparticles: Past, Present, and Future, Langmuir 25 (24) (2009) 13840–13851.
[18] S. Ghadamgahi, J.H. Johnston, C. Fonseca-Paris, Ecofriendly palladium on wool nanocatalysts for cyclohexene hydrogenation, Nanomaterials 8 (8) (2018) 621.
[19] M.K. Erdoğan, Preparation and stabilization of Ag nanoparticles with N-vinyl-2-pyrrolidone grafted-poly (vinyl alcohol) in an organic medium and investigation of their usability in the catalytic dye decolorization, Colloid Interface Sci. Commun. 34 (2020) 100222.
[20] G.A. Tığ, Development of electrochemical sensor for detection of ascorbic acid, dopamine, uric acid and l-tryptophan based on Ag nanoparticles and poly(l-arginine)-graphene oxide composite, J. Electroanal. Chem. 807 (2017) 19–28.
[21] D. Feng, F. Wang, Z. Chen, Electrochemical glucose sensor based on one-step construction of gold nanoparticle–chitosan composite film, Sens. Actuators, B 138 (2) (2009) 539–544.
[22] T. Meng, H. Jia, S. An, H. Wang, X. Yang, Y. Zhang, Pd nanoparticles-DNA layered nanoreticulation biosensor based on target-catalytic hairpin assembly for ultrasensitive and selective biosensing of microRNA-21, Sens. Actuators, B 323 (2020) 128621.
[23] P. Nezhad-Mokhtari, M. Akrami-Hasan-Kohal, M. Ghorbani, An injectable chitosan-based hydrogel scaffold containing gold nanoparticles for tissue engineering applications, Int. J. Biol. Macromol. 154 (2020) 198–205.
[24] D.S. dos Santos, P.J.G. Goulet, N.P.W. Pieczonka, O.N. Oliveira, R.F. Aroca, Gold nanoparticle embedded, self-sustained chitosan films as substrates for surface-enhanced Raman scattering, Langmuir 20 (23) (2004) 10273–10277.
[25] O.S. Adeyemi, F.A. Sulaiman, Evaluation of metal nanoparticles for drug delivery systems, J. Biomed. Res. 29 (2) (2015) 145–149.
[26] G.A. Tığ, G. Günendi, Ş. Pekyardımcı, A selective sensor based on Au nanoparticles-graphene oxidepoly(2,6-pyridinedicarboxylic acid) composite for simultaneous electrochemical determination of ascorbic acid, dopamine, and uric acid, J. Appl. Elechem. 47 (2017) 607–618.
[27] L. Wang, T. Meng, L. Liang, J. Sun, S. Wu, H. Wang, X. Yang, Y. Zhang, Fabrication of amine-functionalized metal-organic frameworks with embedded palladium nanoparticles for highly sensitive electrochemical detection of telomerase activity, Sens. Actuators, B 278 (2019) 133–139.
[28] L. Wang, T. Meng, D. Zhao, H. Jia, S. An, X. Yang, H. Wang, Y. Zhang, An enzyme-free electrochemical biosensor based on well monodisperse Au nanorods for ultra-sensitive detection of telomerase activity, Biosens. Bioelectron. 148 (2020) 111834.
[29] L. Wang, T. Meng, G. Yu, S. Wu, J. Sun, H. Jia, H. Wang, X. Yang, Y. Zhang, A label-free electrochemical biosensor for ultra-sensitively detecting telomerase activity based on the enhanced catalytic currents of acetaminophen catalyzed by Au nanorods, Biosens. Bioelectron. 124–125 (2019) 53–58.
[30] E.Ö. Bolat, G.A. Tığ, Ş. Pekyardımcı, Fabrication of an amperometric acetylcholine esterase-choline oxidase biosensor based on MWCNTs-Fe3O4NPs-CS nanocomposite for determination of acetylcholine, J. Electroanal. Chem. 785 (2017) 241–248.
[31] B. Thirumalraj, N. Dhenadhayalan, S.-M. Chen, Y.-J. Liu, T.-W. Chen, P.-H. Liang, K.-C. Lin, Highly sensitive fluorogenic sensing of L-Cysteine in live cells using gelatin-stabilized gold nanoparticles decorated graphene nanosheets, Sens. Actuators, B 259 (2018) 339–346.
[32] G.A. Tığ, Highly sensitive amperometric biosensor for determination of NADH and ethanol based on Au-Ag nanoparticles/poly (L-cysteine)/reduced graphene oxide nanocomposite, Talanta 175 (2017) 382–389.
[33] H. Hamouche, S. Makhlouf, A. Chaouchi, M. Laghrouche, Humidity sensor based on keratin bio polymer film, Sens. Actuators, A 282 (2018) 132–141.
[34] Y. Gao, S. Gu, F. Jia, G. Gao, A skin-matchable, recyclable and biofriendly strain sensor based on a hydrolyzed keratin-containing hydrogel, J. Mater. Chem. A 8 (45) (2020) 24175–24183.
[35] Y. Gao, S. Gu, F. Jia, Q. Wang, G. Gao, "All-in-one" hydrolyzed keratin protein-modified polyacrylamide composite hydrogel transducer, Chem. Eng. J. 398 (2020) 125555.
[36] M.K. Erdoğan, M. Karakışla, M. Saçak, Improvement of the adhesion of conductive poly (m-toluidine) onto chemically reduced-wool fabrics, Turk. J. Chem. 44 (3) (2020) 775–790.
[37] A. Diamantatos, Spectrophotometric determination of palladium with thioglycolic acid, Anal. Chim. Acta 61 (2) (1972) 233–237.
[38] B. Stypinski-Mis, G. Anderegg, The stability of palladium(II) complexes with sulphur-containing ligands, Anal. Chim. Acta 406 (2) (2000) 325–332.
[39] M. Toskić-Radojicić, Testing keratolytic effect of carbamide in various vehicles, Vojnosanit Pregl 59 (4) (2002) 393–397.
[40] J.A. Maclaren, Maximum extraction of wool proteins by thiol-urea solutions, Text. Res. J. 57 (2) (1987) 87–92.
[41] Y. Yang, Chapter 13 - cys disulfide-related side reactions in peptide synthesis, in: Y. Yang (Ed.), Side Reactions in Peptide Synthesis, Academic Press, Oxford, 2016, pp. 299–310.
[42] C. Leichner, C. Steinbring, R.A. Baus, D. Baecker, R. Gust, A. Bernkop-Schnürch, Reactive keratin derivatives: a promising strategy for covalent binding to hair, J. Colloid Interface Sci. 534 (2019) 533–541.
[43] F. Maestá Bezerra, Ó. García Carmona, C. García Carmona, A.M. Souza Plath, M. Lis, Biofunctional wool using β-cyclodextrins as vehiculizer of citronella oil, Process Biochem. 77 (2019) 151–158.
[44] E. Wojciechowska, A. Włochowicz, A. Wesełucha-Birczyńska, Application of Fourier-transform infrared and Raman spectroscopy to study degradation of the wool fiber keratin, J. Mol. Struct. 511–512 (1999) 307–318.
[45] A. Aluigi, M. Zoccola, C. Vineis, C. Tonin, F. Ferrero, M. Canetti, Study on the structure and properties of wool keratin regenerated from formic acid, Int. J. Biol. Macromol. 41 (3) (2007) 266–273.
[46] J. Zhang, Y. Li, J. Li, Z. Zhao, X. Liu, Z. Li, Y. Han, J. Hu, A. Chen, Isolation and characterization of biofunctional keratin particles extracted from wool wastes, Powder Technol. 246 (2013) 356–362.
[47] W.K. Surewicz, H.H. Mantsch, D. Chapman, Determination of protein secondary structure by Fourier transform infrared spectroscopy: a critical assessment, Biochemistry 32 (2) (1993) 389–394.
[48] C. Tonin, A. Aluigi, C. Vineis, A. Varesano, A. Montarsolo, F. Ferrero, Thermal and structural characterization of poly(ethylene-oxide)/keratin blend films, J. Therm. Anal. Calorim. 89 (2) (2007) 601–608.
[49] J.B. Allen, R.F. Larry, Electrochemical methods fundamentals and applications, John Wiley & Sons, 2001.
[50] Y. Yao, K.-K. Shiu, Electron-transfer properties of different carbon nanotube materials, and their use in glucose biosensors, Anal. Bioanal. Chem. 387 (1) (2007) 303–309.
[51] W. Wang, B. Zhang, Z. He, Bioelectrochemical deposition of palladium nanoparticles as catalysts by Shewanella oneidensis MR-1 towards enhanced hydrogen production in microbial electrolysis cells, Electrochim. Acta 318 (2019) 794–800.
[52] R. Tan, D. Wu, S. Xu, Y. Zhu, D. Xiong, L. Wang, P. Yang, P.K. Chu, Electrocatalytic hydrogen evolution of palladium nanoparticles electrodeposited on nanographene coated macroporous electrically conductive network, Int. J. Hydrogen Energy 43 (4) (2018) 2171–2183.
[53] Y. Zhang, M. Zhang, Z. Cai, M. Chen, F. Cheng, A novel electrochemical sensor for formaldehyde based on palladium nanowire arrays electrode in alkaline media, Electrochim. Acta 68 (2012) 172–177.
[54] D. Fang, L. Yang, G. Yang, G. Yi, Y. Feng, P. Shao, H. Shi, K. Yu, D. You, X. Luo, Electrodeposited graphene hybridized graphitic carbon nitride anchoring ultrafine palladium nanoparticles for remarkable methanol electrooxidation, Int. J. Hydrogen Energy 45 (41) (2020) 21483–21492.
[55] Y. Zhang, J. Ye, Electrochemical sensor based on palladium loaded laser scribed graphitic carbon nanosheets for ultrasensitive detection of hydrazine, New J. Chem. 42 (16) (2018) 13744–13753.

[56] H. Zhan, J. Li, Z. Liu, Y. Zheng, Y. Jing, A highly sensitive electrochemical OP biosensor based on electrodeposition of Au–Pd bimetallic nanoparticles onto a functionalized graphene modified glassy carbon electrode, Anal. Methods 7 (9) (2015) 3903–3911.
[57] P. Bartlett, C. Toh, E. Calvo, V. Flexer, Modelling biosensor responses, Wiley, Chichester, England, 2008.
[58] L.V. Sigolaeva, T.V. Bulko, M.S. Kozin, W. Zhang, M. Köhler, I. Romanenko, J. Yuan, F.H. Schacher, D.V. Pergushov, V.V. Shumyantseva, Long-term stable poly(ionic liquid)/MWCNTs inks enable enhanced surface modification for electrooxidative detection and quantification of dsDNA, Polymer 168 (2019) 95–103.
[59] Q. Yang, Z. Quan, B. Du, S. Wu, P. Li, Y. Sun, Z. Lei, X. Wang, Wool-anchored Pd (OAc)2 complex: a highly active and reusable catalyst for desulfurative coupling reactions, Catal. Sci. Technol. 5 (9) (2015) 4522–4531.
[60] A.B. Yousaf, M. Imran, M. Farooq, P. Kasak, Interfacial phenomenon and nanostructural enhancements in palladium loaded lanthanum hydroxide nanorods for heterogeneous catalytic applications, Sci. Rep. 8 (1) (2018) 1–9.
[61] H. Zhang, H. Yan, N. Mao, Functional modification with TiO2 nanoparticles and simultaneously dyeing of wool fibers in a one-pot hydrothermal process, Ind. Eng. Chem. Res. 53 (5) (2014) 2030–2041.
[62] J. Yu, T.H. Kim, A facile electrochemical fabrication of reduced graphene oxide-modified glassy carbon electrode for simultaneous detection of dopamine, ascorbic acid, and uric acid, J. Electrochem. Sci. Technol. 8 (4) (2017) 274–281.